Physica D 239 (2010) 504–514

Contents lists available at ScienceDirect

Physica D

journal homepage: www.elsevier.com/locate/physd

Singular Hopf bifurcations and mixed-mode oscillations in a two-cell inhibitory neural network

Rodica Curtu

Department of Mathematics, University of Iowa, 14 MacLean Hall, Iowa City, IA 52242, United States

ARTICLE INFO

Article history:
Available online 4 January 2010

Keywords:
Neural systems
Mixed-mode oscillations
Canards
Singular Hopf
Double-homoclinics
Period-doubling and Neimark–Sacker bifurcations

ABSTRACT

Recent studies of a firing rate model for neural competition as observed in binocular rivalry and central pattern generators [R. Curtu, A. Shpiro, N. Rubin, J. Rinzel, Mechanisms for frequency control in neuronal competition models, SIAM J. Appl. Dyn. Syst. 7 (2) (2008) 609–649] showed that the variation of the stimulus strength parameter can lead to rich and interesting dynamics. Several types of behavior were identified such as: fusion, equivalent to a steady state of identical activity levels for both neural units; oscillations due to either an *escape* or a *release* mechanism; and a winner-take-all state of bistability. The model consists of two neural populations interacting through reciprocal inhibition, each endowed with a slow negative-feedback process in the form of spike frequency adaptation. In this paper we report the occurrence of another complex oscillatory pattern, the mixed-mode oscillations (MMOs). They exist in the model at the transition between the relaxation oscillator dynamical regime and the winner-take-all regime. The system distinguishes itself from other neuronal models where MMOs were found by the following interesting feature: there is no autocatalysis involved (as in the examples of voltage-gated persistent inward currents and/or intrapopulation recurrent excitation) and therefore the two cells in the network are *not* intrinsic oscillators; the oscillations are instead a combined result of the mutual inhibition and the adaptation. We prove that the MMOs are due to a *singular* Hopf bifurcation point situated in close distance to the transition point to the winner-take-all case. We also show that in the vicinity of the singular Hopf other types of bifurcations exist and we construct numerically the corresponding diagrams.

1. Introduction

Mixed-mode oscillations (MMOs) were observed in both experiments and models of systems from chemistry [1–7], physics [8,9] and neuroscience [10–16], and they are defined as complex oscillatory patterns consisting of small amplitude oscillations followed by large excursions of relaxation type, in each periodic cycle. For example, localized structures of large amplitude oscillations on a background of small amplitude oscillations were identified in experiments on the photosensitive $Ru(bpy)_3$-catalyzed Belousov–Zhabotinsky reaction in a thin layer of silica gel with photochemical global negative feedback imposed through illumination [5]; in the neural system, MMOs were found in central pattern generators such as the lower brain stem network (the pre-Bötzinger complex) that generates respiratory rhythm in mammals [11], or in electrophysiological (in vitro) studies of spiny stellate cells in layer II medial entorhinal cortex [10]; more recently, MMOs were also discovered in dusty plasmas [9].

What are the functional consequences of the MMOs in these chemical, physical and biological systems is still an open question, as well as is the understanding of the underlying mechanisms that produce them.

The number, amplitude and shape of small and large excursions in MMOs may vary depending on the specific structure of the system (and so, on the mechanism leading to MMOs) and on the values of certain parameters. Using techniques from dynamical systems and bifurcations theory, several distinct mechanisms have been proposed to explain the occurrence of MMOs such as break-up (loss) of stability of a Shilnikov homoclinic orbit [17,18], break-up of an invariant torus [19], subcritical Hopf-homoclinic bifurcation [20], a (generalized, folded node type) canard phenomenon [21–24], and, more recently, a *singular Hopf* bifurcation [25].

In particular, the last two mechanisms are associated with multiple-timescale dynamical systems. A common feature is that the slow stable and unstable manifolds of the system (situated exponentially close to the critical manifold) play an important role in the generation of MMOs as they are involved in both the definition of the global return map that corresponds to the large relaxation-like excursion, and in the generation of small amplitude oscillations. The intersection between the slow stable and slow unstable manifolds (named the *curve of folds* or, simply, *the fold*) is especially of interest.

E-mail address: rodica-curtu@uiowa.edu.

0167-2789/$ – see front matter © 2009 Elsevier B.V. All rights reserved.
doi:10.1016/j.physd.2009.12.010

The distinction between a (folded node type) canard generated MMO and a singular Hopf generated MMO comes mainly from the following fact: in the former case there is no equilibrium point of the original system in the neighborhood where the small (subthreshold) oscillations occur, while in the latter there is. The theory has been developed for systems with at least one fast and at least two slow variables since that guarantees that the solutions are generic [25,26].

In the first case, the folded node is an equilibrium of the desingularized flow on the critical manifold but *not* an equilibrium of the original fast–slow system. The folded node belongs to the fold. A whole family of solutions crosses via the folded node singularity from the attracting to the repelling branch of the slow manifold. The folded node possesses a unique (strong) canard and non-unique (weak/secondary) canards which delineate a trapping region (a funnel). Then any solution that ends up in the funnel passes near the folded node singularity and, consequently, experiences a delay; the delay is due to the rotational properties of canards with the primary weak canard having the role of the rotational axis [26].

In the singular Hopf case, an equilibrium of the original fast–slow system exists in the neighborhood of the curve of folds. In fact, a Hopf bifurcation point is on the critical manifold but displaced from the fold by $\mathcal{O}(\varepsilon)$-distance. Then the intersections of the stable and unstable manifolds of this equilibrium point together with those of the slow (stable and unstable) manifolds contribute to the generation of MMOs [25,27].

In a recent paper, Guckenheimer [25] opens an interesting discussion and direction for future research about the differences in the characteristics of MMOs due to singular Hopf points and those created through canards at folded nodes: for example, it seems that in the case of singular Hopf the small oscillations of MMOs start with very low amplitude, then grow slowly before entering the relaxation oscillator phase. In the case of folded nodes, the small oscillations of MMOs decrease and then increase in amplitude, usually with the same number of cycles.

We should mention though that even in the case of the singular Hopf, it is possible that a folded node still exists; nevertheless this folded node is there because a parameter of the system varies close to a value where a *folded saddle–node type II singularity* occurs. The folded saddle–node type II singularity corresponds to a transcritical bifurcation where the Hopf point crosses the curve of folds [25,27,28]. That might explain why, in the literature, some models with MMOs that were associated to folded node canards exhibit only the increasing-in-amplitude small oscillations but not the decreasing-in-amplitude ones (see for example [16]).

Mixed-mode oscillations in a two-cell inhibitory neural network. We investigate in this paper the existence of MMOs in a neural system with two fast and two slow variables and show that they are associated with a singular Hopf bifurcation. The system models competition between two populations of neurons and has been used to describe perceptual bistability due to ambiguous external stimuli [29–31], or, in a slightly modified form, for central pattern generators [32–34]. For example, binocular rivalry (a classical example of perceptual bistability) is experienced by a person when his/her eyes are exposed simultaneously to two significantly different images. Over a large range of stimulus conditions, the person reports an alternation between the two competing percepts (images) as opposed to a mixture of them. The alternation is therefore called perceptual *rivalry*. In modeling terms, the alternation corresponds on average to an anti-phase periodic solution; competition is implemented via reciprocal inhibition that acts effectively as a fast positive feedback (disinhibition); in addition, a slow negative-feedback process is assumed and it is associated to either the spike frequency adaptation or to the synaptic depression.

A very interesting feature of this model is that its oscillations (simple and/or mixed-mode) are a consequence of *both* coupling and local feedback. In other words, the two cells (populations) in the network are *not* intrinsic oscillators; in fact it can be proved that, once decoupled (see (1) in Section 2 with $\beta = 0$), the only possible state of each cell is the equilibrium [30]. This property distinguishes the system we investigate here from other neuronal models where MMOs were found: coupled-oscillators [12,13,23] or neuron models involving autocatalysis in either an intrinsic process form (like voltage-gated persistent inward currents) or as synaptic process (like intrapopulation recurrent excitation) [14–16,24]. There is no autocatalysis in this two-cell competition network, the alternation being in fact a combined result of mutual inhibition and adaptation. That has direct implications on the return mechanism (large amplitude excursions) involved in the formation of MMOs [27].

Moreover, compared with the models mentioned above, system (1) is relatively simple and so it has the advantage of being tackled much easily with analytical methods. In the following sections we identify and characterize analytically the conditions for a singular Hopf bifurcation to exist at nontrivial equilibria and we construct the associated normal form (Section 3.2). Once the normal form is determined, we use it to explain the existence of MMOs at the transition between rivalry oscillation and winner-take-all dynamical regimes (Section 4). In addition, we numerically investigate the phase space of (1) close to the transition point and identify here several interesting limit point sets (Section 2.1).

2. Model description and numerical investigation

The two-cell (two-population) inhibitory neural network with adaptation that we study in this paper is modeled by a four-dimensional system of ordinary differential equations,

$$\begin{aligned}
\frac{\mathrm{d}u_1}{\mathrm{d}t} &= -u_1 + S(I - \beta u_2 - g a_1),\\
\frac{\mathrm{d}u_2}{\mathrm{d}t} &= -u_2 + S(I - \beta u_1 - g a_2),\\
\tau\frac{\mathrm{d}a_1}{\mathrm{d}t} &= -a_1 + u_1,\\
\tau\frac{\mathrm{d}a_2}{\mathrm{d}t} &= -a_2 + u_2,
\end{aligned} \tag{1}$$

where $\tau \gg 1$ and S is a nonlinear gain function of inverse $F = S^{-1}$. The function S satisfies certain conditions such as being differentiable, monotonically increasing from $\lim_{x\to-\infty} S(x) = 0$ to $\lim_{x\to\infty} S(x) = 1$ and with convexity-change (from concave-up to concave-down) at some given value $x = \theta$ (Fig. 1A). Let us define u_0 as the value the function S takes at θ, that is $u_0 = S(\theta)$. Then the following conditions are true for the inverse function F: $\lim_{u\to 0} F'(u) = \lim_{u\to 1} F'(u) = \infty$, $F''(u) < 0$ for $u \in (0, u_0)$, $F''(u) > 0$ for $u \in (u_0, 1)$, $F''(u_0) = 0$ (see the graph of F' in Fig. 1B). The typical gain function is the sigmoid and it depends on two parameters (positive r and real θ) that control the slope and the activation threshold,

$$S(x) = \frac{1}{1 + \mathrm{e}^{-r(x-\theta)}}. \tag{2}$$

Each fast equation is associated with one population of neurons and describes the time evolution of its spatially averaged firing rate (u_j, $j = 1, 2$); each slow equation monitors the (slow) time fatigue accumulation (a_j, $j = 1, 2$); competition is achieved through mutual inhibition of strength β and negative feedback (such as spike frequency adaptation) of strength g; in addition, each population receives external stimulation of equal strength I (β, g and I are all positive parameters).

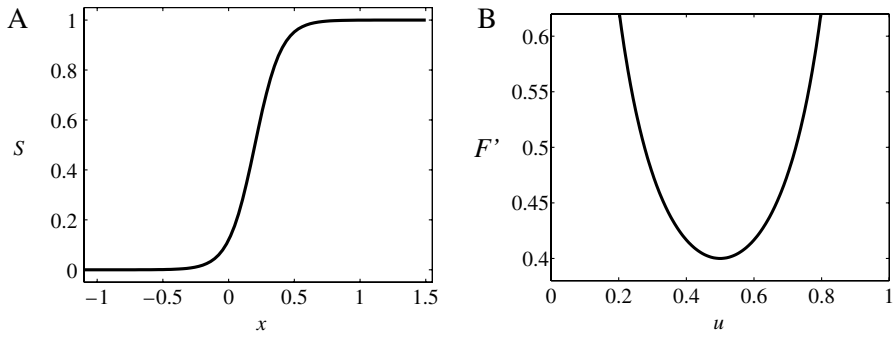

Fig. 1. (A) Nonlinear gain function S. (B) The graph of the first derivative F' of inverse function $F = S^{-1}$ has a well shape with vertical asymptotes at 0 and 1, and it is always positive.

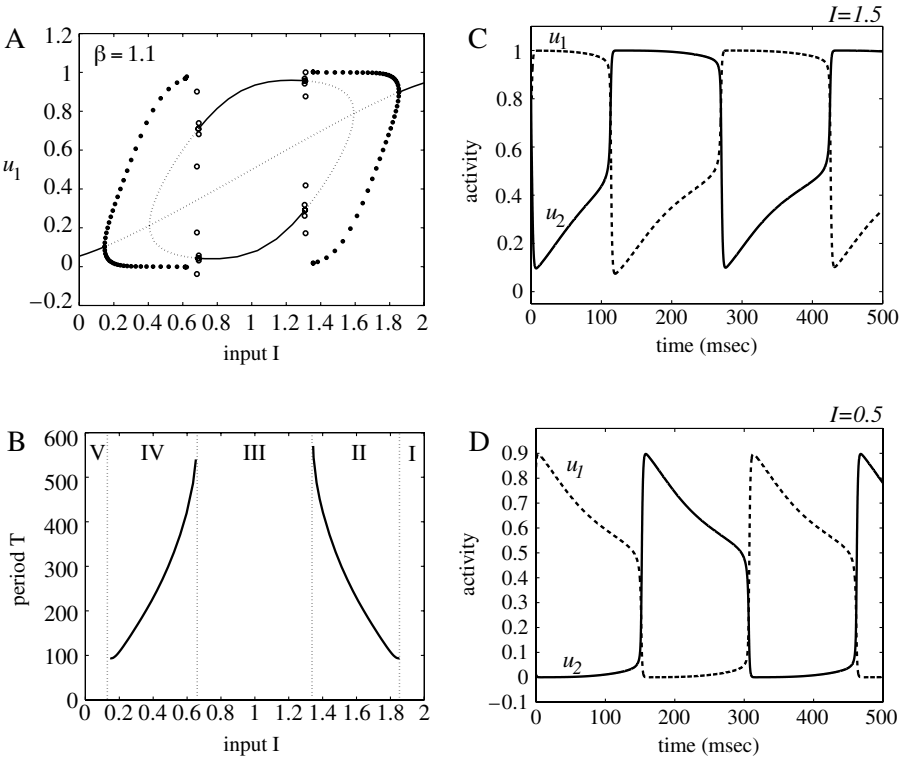

Fig. 2. (A, B) Numerical bifurcation diagrams for system (1) and (C, D) examples of activity timecourses $u_1(t)$, $u_2(t)$ for parameters $\beta = 1.1, g = 0.5, r = 10$ and $\theta = 0.2$. The slow timescale of the adaptation variables is $\tau = 100$. An obvious difference between regions II and IV in the bifurcation diagram of period T versus input I is that oscillations obtained through an escape mechanism have longer period with decreased values for I ((B): region II and (C) timecourses at $I = 1.5$), while those due to a release mechanism have longer period for increased values of I ((B): region IV and (D) timecourses at $I = 0.5$).

Previous studies [30,31] show that system (1)'s dynamical properties change with input I from: (i) fusion at identically high levels of activity (one attractive steady state with $u_1 = u_2$; region I in Fig. 2A–B) to (ii) anti-phase oscillation due to an escape mechanism (region II in Fig. 2A–B; see also Fig. 2C for timecourses of $u_1(t)$ and $u_2(t)$ at $I = 1.5$); (iii) a winner-take-all behavior due to the existence of two bistable equilibria with $u_1 \neq u_2$ (region III, Fig. 2A–B); (iv) anti-phase oscillation due to a release mechanism (region IV in Fig. 2A–B and D with timecourses of $u_1(t)$ and $u_2(t)$ at $I = 0.5$); and (v) fusion at identically low levels of activity (again one single attractive steady state with $u_1 = u_2$; region V in Fig. 2A–B). Note that in biological terms *fusion*, for example, would represent a steady state of the network in which both population activities stabilize at the same level, that is $u_1 = u_2$. Since the network reaches an equilibrium, the slow variables become constant as well, and due to the form of equations that describe their time evolution they asymptotically approach the activity levels ($a_1 = u_1$ and $a_2 = u_2$); therefore once the transients are ignored, all variables are equal. On the other hand, the *winner-take-all* dynamics corresponds to the case when one neural population remains active (dominant) and the other inactive (suppressed) indefinitely and so the switching between states does not take place anymore. Mathematically, this is also a steady state but with u_1 and u_2 distinct ($a_1 = u_1 \neq u_2 = a_2$).

We summarize these properties in the numerical bifurcation diagrams from Fig. 2 for the choice of parameters: $\beta = 1.1, g = 0.5, r = 10, \theta = 0.2, \tau = 100$ and $I = 1.5$ and 0.5 respectively. For a given value of I, stable (unstable) equilibria are represented by thick (dashed) lines (Fig. 2A); similarly, branched circle-curves correspond to the maximum and minimum amplitudes of the oscillatory solutions and they are drawn as filled-circles (open-circles) for stable (unstable) cycles. An obvious difference between regions II and IV is that the oscillations obtained through an escape mechanism have longer period for decreased values of I (e.g. region II in Fig. 2B), while those due to a release mechanism have longer period for increased values of I (e.g. region IV in Fig. 2B). The terms

escape and *release* were introduced and defined in the context of neuronal competition models in [30] and they refer to the main cause of the switch. During oscillation, the two neural populations take turn in being active. If u_1 is dominant then its negative feedback a_1 accumulates and the net input $I-\beta u_2-ga_1$ decreases; on the other hand, the feedback a_2 decays for the suppressed population u_2 and its net input $I-\beta u_1-ga_2$ increases. The high nonlinearity in gain function S comes now into play and transforms equal changes in the net input of both populations into significantly different effective responses $S(I-\beta u_2-ga_1)$ and $S(I-\beta u_1-ga_2)$. The switch is triggered by either the (more abrupt) change in the response to an input to the suppressed population, or to the change in the input response to the dominant population. The former means that the suppressed population changes faster, regains control and pushes its competitor down and therefore it is called an *escape* mechanism. The latter means that the activity of the dominant population drops faster and so becomes inefficient in suppressing its competitor which becomes active; this case is called a *release* mechanism.

The bifurcation diagram of activity u_j versus input I from Fig. 2A is valid under the following assumptions: (i) the neural network (1) is adaptation/negative feedback dominated instead of inhibition/coupling dominated, that is $\beta < g(\tau+1)$, and (ii) the inhibition has sufficiently strong strength $\beta > \frac{1+1/\tau}{S'(\theta)}$. Moreover, multiple equilibria occur if β is at least $\beta > g+1/S'(\theta)$ and winner-take-all bistability appears for $\beta > \beta_{wta}$ for some value β_{wta} that can be analytically estimated (e.g. see formula (4.11) in [30]).

The transition between fusion and oscillatory dynamics (regions I and II, or V and IV) is well-understood and is due to a supercritical Hopf bifurcation at the trivial equilibrium $\mathbf{e}_I = (u_I, u_I, u_I, u_I)$. The bifurcation diagram indicates also a subcritical Hopf as reason for the change in stability of the nontrivial steady states $\mathbf{e}_{sI} = (u_{1I}, u_{2I}, u_{1I}, u_{2I})$ and $\mathbf{e}_{iI} = (u_{2I}, u_{1I}, u_{2I}, u_{1I})$ and occurrence of winner-take-all behavior. However it is still unclear how the stable limit cycle disappears.

Let us notice that the symmetry of the bifurcation diagram with respect to input parameter I is a direct consequence of the symmetry of system (1) itself [30]. Therefore it is sufficient to understand the mechanism of dynamical transition from, say, regions II to III in system (1) because the same argument will apply to the transition between IV and III. These are precisely the ranges of the input values I where MMOs were numerically detected and we will focus our attention on them.

2.1. Numerical simulations and bifurcation diagrams

We begin our study of the mechanism responsible for the change from relaxation–oscillation to the winner-take-all behavior in system (1), by zooming in the range of parameter values I close to the transition point. We will mainly focus on the change between regimes II and III from Fig. 2A, since its symmetric case (IV and III) is similar.

An appropriate adjustment (scaling) of the parameters helps us magnify the transitional region and offers a very good perspective. For example, the bifurcation diagram obtained for $\beta=2.5, g=1.5, r=10, \theta=0.2$ and $\tau=5$ shows a supercritical Hopf point at I_{HB}, a pitchfork bifurcation point at I_{BP} and two simultaneous subcritical Hopf points at I_{sHB} (Fig. 3). At I_{HB} a stable limit cycle of period $T=19.48$ emerges from the trivial equilibrium $\mathbf{e}_I$; at I_{BP} two additional steady states $\mathbf{e}_{sI}$ and $\mathbf{e}_{iI}$ emerge; at I_{sHB} the nontrivial branches of solutions change stability and in both cases an unstable limit cycle is born.

In order to facilitate the description of the changes that occur in the system's dynamics under stimulus strength variation, we include in Table 1 a list of all parameter I significant values (e.g. $I_{HB}=4.291$, $I_{BP}=3.956$ and so forth). Each of these values corresponds to a bifurcation point that is explicitly defined in the table; trajectories resulting at the bifurcation points are then numerically constructed in the (u_1, a_1, I) space and illustrated in Figs. 4–6. We used XPPAUT [35,36] to draw the bifurcation diagram (Fig. 3) and then MATCONT [37] to draw several important trajectories (Figs. 4–6).

Table 1
Significant bifurcation points in a two-cell inhibitory neural network.

I	Bifurcation type	Figs.
$I_{HB}=4.291$	Supercritical Hopf at equilibrium $\mathbf{e}_I$	3 and 4
$I_{BP}=3.956$	Subcritical pitchfork at equilibrium $\mathbf{e}_I$	3
$I_{\mathcal{NS}}=3.7095$	Neimark–Sacker	4 and 5
$I_{\mathcal{PD}}=3.6964$	Period-doubling	5
$\tilde{I}=3.693$	Cascade of NS and PD	5
$I_{HL}=3.639$	Double-homoclinic at $\mathbf{e}_I$	3 and 6A
$I_{sHB}=3.569$	Subcritical Hopf at $\mathbf{e}_{iI}$ (and $\mathbf{e}_{sI}$)	3 and 6B
$I_{NS}=3.5437$	Neimark–Sacker	6
$I_{PD}=3.54303$	Period-doubling	6
$I_{LPC}=3.54299$	Saddle–node of (unstable) limit cycles	3 and 6

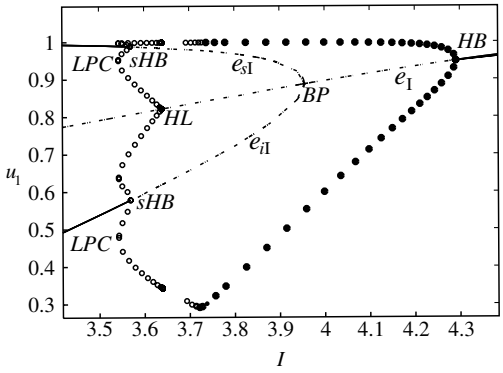

Fig. 3. Bifurcation diagram of the neural system (1) for a range of values I that illustrates fusion, oscillation and winner-take-all dynamics. Other parameters are $\beta=2.5, g=1.5, \tau=5, r=10$ and $\theta=0.2$. The stable relaxation oscillator born at $I_{HB}=4.291$ from the trivial equilibrium $\mathbf{e}_I$ loses its stability at about $\tilde{I}=3.693$. At $I_{sHB}=3.569$ an unstable limit cycle is born at each nontrivial equilibrium ($\mathbf{e}_{iI}$ and $\mathbf{e}_{sI}$) and it merges with another unstable cycle at $I_{LPC}=3.54299$ through a saddle–node for limit cycle bifurcation. The additional unstable cycle appeared from a homoclinic bifurcation at $I_{HL}=3.639$. In fact, due to the symmetry of the system, at I_{HL}, a double-homoclinic exists.

The stable limit cycle that exists for values of I close to (and smaller than) I_{HB} corresponds to an oscillation of both activity variables u_1 and u_2 in the two-cell inhibitory network (1). The cycle appears at I_{HB} with relatively constant period $T\approx 19.48$ but close to zero amplitude, and it changes for I near I_{HB} into a relaxation oscillator (that is an oscillation of large amplitude with fast transitions between an active and a silent phase); the period of oscillation increases with decreasing I (Fig. 5). Variables u_1 and u_2 are phase-locked in anti-synchrony and take turn in being dominant. Their trace as a function of time is similar to the trajectories in Fig. 2C obtained for $\tau=100$ but, as expected here, their dominance period is adjusted to (proportional to) $\tau=5$. The slow varying variables a_1 and a_2 oscillate as well in anti-phase but opposed to u_1, u_2 they do not experience any sudden jump (not shown). A numerical continuation of the stable limit cycle born at the supercritical Hopf I_{HB} is constructed in Fig. 4. The limit cycle goes through a Neimark–Sacker bifurcation at $\tilde{I}_{\mathcal{NS}}=3.7095$ and becomes unstable; then at $\tilde{I}_{\mathcal{PD}}=3.6964$ a period-doubling bifurcation is detected and it is followed by a cascade of Neimark–Sacker and period-doubling points close to $\tilde{I}$ (Figs. 4 and 5).

The point $\mathbf{e}_I$ corresponds to the case when both cells in the network have constant and equal activity values, $u_1=u_2$ (after the time-transients are discarded). Since the network is at equilibrium

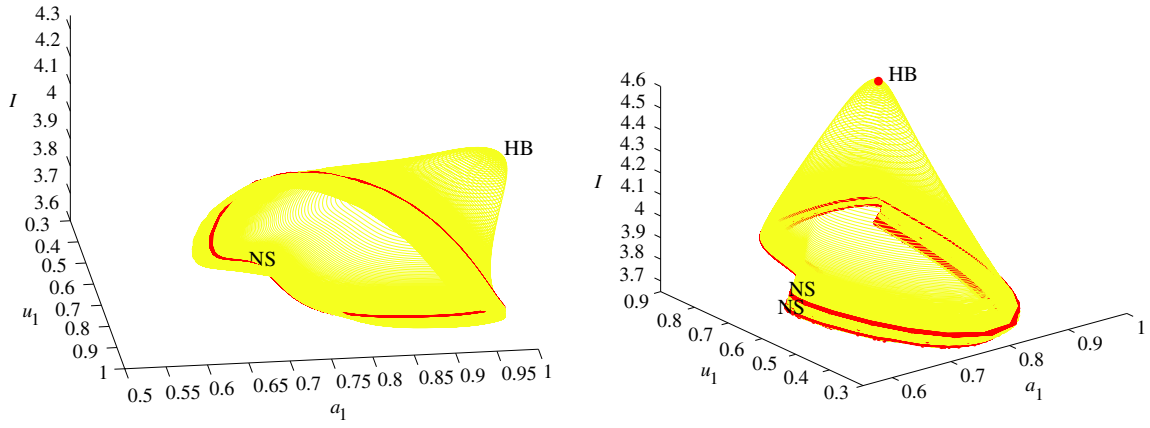

Fig. 4. Continuation of the stable limit cycle born at the supercritical Hopf ($I_{HB} = 4.291$) for $I < I_{HB}$. A Neimark–Sacker point is detected at $I_{\mathcal{NS}} = 3.7095$ and the limit cycle becomes unstable.

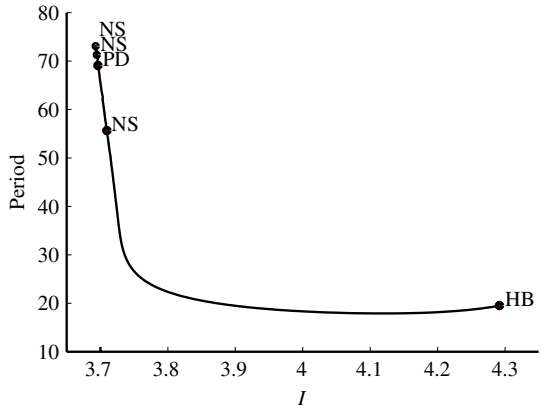

Fig. 5. The period of oscillation for the stable limit cycle born at $I_{HB} = 4.291$ increases as the stimulus strength I is decreased. The cycle undergoes a Neimark–Sacker bifurcation at $I_{\mathcal{NS}} = 3.7095$, a period-doubling bifurcation at $I_{\mathcal{PD}} = 3.6964$ and then a cascade of Neimark–Sacker points close to $\tilde{I} = 3.693$ where the continuation fails.

the slow variables a_1 and a_2 reach a constant level themselves and, according to their equations in (1), they satisfy $a_1 = u_1$ and $a_2 = u_2$. For this reason we call $\mathbf{e}_I$ a *trivial* equilibrium; for large I it is the only attractor of the system (1) but it loses stability at I_{HB} when the trajectories enter the oscillatory regime described above.

At I_{BP} two nontrivial equilibrium points $\mathbf{e}_{iI}$ and $\mathbf{e}_{sI}$ emerge from the trivial equilibrium $\mathbf{e}_I$. It can be shown that this is a subcritical pitchfork bifurcation [30] and that all equilibrium points are unstable. Due to the multidimensionality of the eigenspace, $\mathbf{e}_I$ does not change its stability when one of its eigenvalues becomes zero; instead it switches from an equilibrium with two-dimensional stable and unstable eigenspaces to a three-dimensional stable and a one-dimensional unstable eigenspaces. The newly born equilibria $\mathbf{e}_{iI}$ and $\mathbf{e}_{sI}$ are also unstable because they inherit the number of unstable modes from their "parent"-equilibrium. Therefore the parameter change at I_{BP} does not introduce any additional attractors in system (1).

Nevertheless these three equilibrium points play a significant role in the global dynamics of (1) as I approaches I_{sHB}. At about $I_{HL} = 3.639$ a pair of unstable oscillatory solutions appear through a double-homoclinic from $\mathbf{e}_I$ (Figs. 3 and 6A). Each of those limit cycles encompasses one of the two nontrivial points $\mathbf{e}_{sI}$ or $\mathbf{e}_{iI}$ respectively and acts as a separatrix in the phase space. Then at I_{sHB} a simultaneous subcritical Hopf bifurcation occurs at $\mathbf{e}_{iI}$ and $\mathbf{e}_{sI}$ and another pair of unstable oscillations appear. These two solutions collide with the former and disappear at $I_{LPC} = 3.54299$ (a saddle–node of limit cycles bifurcation; Figs. 3 and 6B). Numerically we detect some additional bifurcation points in system (1) just before the collision of cycles: a Neimark–Sacker bifurcation at $I_{NS} = 3.5437$ and a period-doubling bifurcation at $I_{PD} = 3.54303$ (Figs. 3 and 6B).

At I_{sHB} the two nontrivial equilibria change their stability properties and become attractors in a range of parameter I with $I < I_{sHB}$. Depending on the initial conditions, trajectories in the phase space are attracted to either $\mathbf{e}_{iI}$ and $\mathbf{e}_{sI}$; therefore this is exactly the winner-take-all case discussed in Section 2.

What are the attractors of the system in the interval $I_{sHB} < I < \tilde{I}$ remains however an open question. Numerical simulations of the neural system (1) for values of I taken passed the double-homoclinic point (I between I_{sHB} and I_{HL}) uncover complex oscillatory patterns that combine small amplitude (subthreshold) oscillations with large excursions of relaxation type (e.g. Fig. 7A for $I = 3.579$ or Fig. 7B for $I = 3.6$). We prove the existence of the mixed-mode oscillations in connection with a singular Hopf point I^* and we detect it in $\mathcal{O}(\frac{1}{\tau})$-distance to the subcritical Hopf point I_{sHB}.

3. Singular Hopf bifurcations and reduction to the normal form

3.1. Preliminaries

In the following we study the system (1) dynamics for input parameter I close to the subcritical Hopf point (Fig. 3). We are interested in the range $I > I_{sHB}$ where equilibria $\mathbf{e}_{iI}$ and $\mathbf{e}_{sI}$ are unstable and MMOs were numerically detected. We will prove analytically that the subcritical Hopf point exists and use its local normal form to explain the creation of MMOs.

Our strategy is to show that there exists a singular Hopf point $(u_1^*, u_2^*, a_1^*, a_2^*)$ at I^* in system (1); then by singular perturbation arguments, we will gain insight into the typical trajectories close to I_{sHB}. Let us consider first the equivalent system to (1) obtained after rescaling time with $\varepsilon = 1/\tau$. The point I^* is called *singular* because the linearization of this system at equilibria close to $(u_1^*, u_2^*, a_1^*, a_2^*)$ and with I close to I^* admits a pair of eigenvalues with singular imaginary parts; that is, eigenvalues $\mu_{1,2} = \phi \pm i\psi$ with $\phi = \phi(\varepsilon) = \mathcal{O}(1)$ and $\psi = \psi(\varepsilon) \to \infty$ as $\varepsilon \to 0$.

We apply the theory developed by Braaksma [38] to system (1). For this, let us summarize below the main results necessary to tackle our problem.

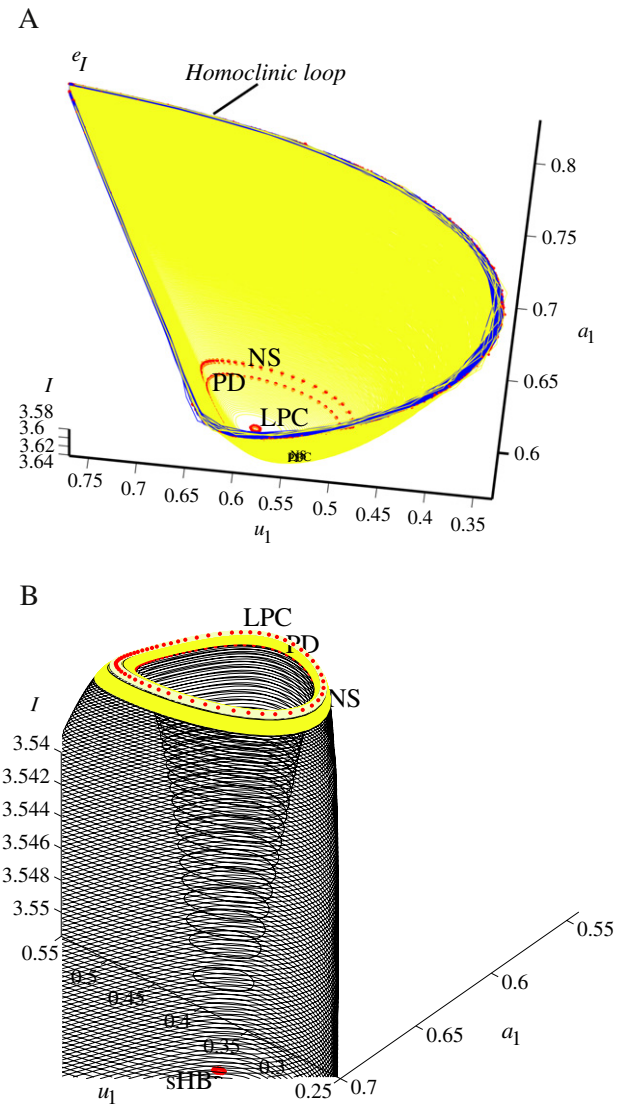

Fig. 6. (A) An unstable limit cycle is born through a homoclinic bifurcation to the saddle $\mathbf{e}_I$ at $I_{HL} = 3.639$. It acts as separatrix between the basins of $\mathbf{e}_I$ and $\mathbf{e}_{II}$. It goes through a Neimark–Sacker bifurcation ($I_{NS} = 3.5437$) and then a period-doubling bifurcation ($I_{PD} = 3.54303$) before it merges at $I_{LPC} = 3.54299$ with an unstable orbit formed at a subcritical Hopf point (see B); (B) two unstable cycles around nontrivial equilibrium $\mathbf{e}_{II}$. They were born through a subcritical Hopf at $I_{sHB} = 3.569$ and a homoclinic bifurcation (see A) respectively, and they merge at I_{LPC} through a saddle–node for cycles.

Proposition 1 (*Braaksma 1998, [38]*). *Let U be an open subset of $\mathbb{R}^m \times \mathbb{R}^n \times \mathbb{R}$ and let $f : U \to \mathbb{R}^m$, $h : U \to \mathbb{R}^n$ be sufficiently smooth functions depending on the parameter b, $f = (f_1, f_2, \ldots, f_m)^T$ and $h = (h_1, h_2, \ldots, h_n)^T$ where T stands for the transpose. Let $(\bar{x}, \bar{y}, \bar{b}) \in U$ be a point where the following conditions on f, h and their derivatives hold (the bar notation denotes functions evaluated at the given equilibrium):*

[N0] *The Jacobian matrix $\bar{f}_x$ is in real Jordan form,*

[N1-3] $\bar{f} = 0, \bar{h} = 0, det \begin{pmatrix} \bar{f}_x & \bar{f}_y \\ \bar{h}_x & \bar{h}_y \end{pmatrix} \neq 0$

[N4-6] $(\bar{f}_m)_{x_m} = 0, (\bar{f}_m)_y \bar{h}_{x_m} < 0, (\bar{f}_m)_{x_m x_m} \neq 0,$

[N7] $\chi \neq 0$ *where* $\chi = -\begin{pmatrix} (\bar{f}_m)_{x_m x} & (\bar{f}_m)_{x_m y} \end{pmatrix} \begin{pmatrix} \bar{f}_x & \bar{f}_y \\ \bar{h}_x & \bar{h}_y \end{pmatrix}^{-1} \begin{pmatrix} \bar{f}_b \\ \bar{h}_b \end{pmatrix} + (\bar{f}_m)_{x_m b}.$

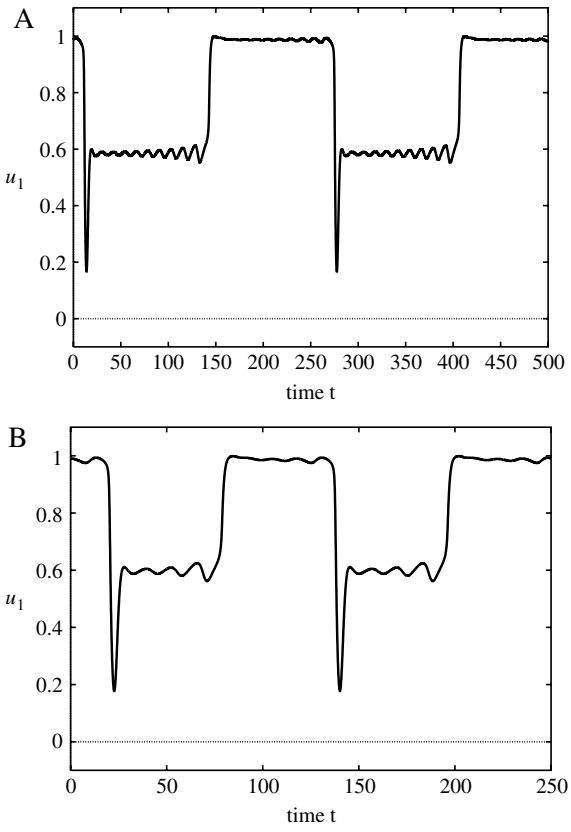

Fig. 7. Mixed-mode oscillations in the two-cell inhibitory neural system for $\beta = 2.5, g = 1.5, r = 10, \theta = 0.2, \tau = 5$ and (A) $I = 3.579$; (B) $I = 3.6$. Note that the closer I is to the bifurcation point ($I_{sHB} = 3.569$), the longer the time spent on small amplitude oscillations around each nontrivial equilibrium (for example in (A); the timescale is in the order of hundreds while $\tau = 5$).

Note that we use here the following matrix notation: $f_x := \left(\frac{\partial f_i}{\partial x_j}\right)_{i,j}$, $f_y := \left(\frac{\partial f_i}{\partial y_k}\right)_{i,k}$, $(f_m)_y := \left(\frac{\partial f_m}{\partial y_k}\right)_k$, $h_{x_m} := \left(\frac{\partial h_k}{\partial x_m}\right)_k$, $f_b := \left(\frac{\partial f_i}{\partial b}\right)_i$, $h_b := \left(\frac{\partial h_k}{\partial b}\right)_k$ *and so forth, with* $i, j = 1, \ldots, m$ *and* $k = 1, \ldots, n$.

Then the system

$$\varepsilon \frac{dx}{dt} = f(x, y, b), \qquad \frac{dy}{dt} = h(x, y, b) \tag{3}$$

with $0 < \varepsilon \ll 1$ *can be reduced to the following normal form*

$$\begin{aligned} \delta\dot{\xi} &= E(u, \xi) + \mathscr{O}(\delta), \\ \dot{u} &= v + \frac{1}{2}u^2 + \delta\mathscr{F}(u, w, \xi; \lambda) + \mathscr{O}(\delta^2), \\ \dot{v} &= -u + \mathscr{O}(\delta^2), \\ \dot{w} &= \delta H(u, w) + \mathscr{O}(\delta^2), \end{aligned} \tag{4}$$

with $\delta = \mathscr{O}(\sqrt{\varepsilon})$ *and* $\xi \in \mathbb{R}^{m-1}$, $u, v, \lambda \in \mathbb{R}$, $w \in \mathbb{R}^{n-1}$. *The dots denote differentiation with respect to the slow time variable* $t_{slow} = \delta^{-1}t$. *The functions* $E, \mathscr{F}, H$ *have the structure* $E = E_\xi \xi + \frac{1}{2}E_{uu}u^2$, $\mathscr{F} = \lambda u + \mathscr{F}_{u\xi}u\xi + \mathscr{F}_{uw}uw + \frac{1}{6}\mathscr{F}_{uuu}u^3$ *and* $H = H_w w + \frac{1}{2}H_{uu}u^2$, *and their coefficients can be expressed in terms of derivatives of* f *and* h *at* $(\bar{x}, \bar{y}, \bar{b})$. *The constant matrices* E_ξ *and* H_w *are invertible. The coefficient* λ *of* u *in* $\mathscr{F}$ *is the bifurcation parameter and depends on the difference* $(b - \bar{b})$; *as* λ *crosses zero, the linearization of the* (u, v)*-subsystem has a pair of purely imaginary eigenvalues at the origin. The normal form is valid in an* $\mathscr{O}(\sqrt{\varepsilon})$ *neighborhood of* $\bar{x}_m$ *and in an* $\mathscr{O}(\varepsilon)$ *neighborhood of* $\bar{x}_1, \ldots, \bar{x}_{m-1}, \bar{y}, \bar{b}$.

Proposition 2 (*Braaksma 1998, [38]*). *Consider system (3), satisfying the assumptions of Proposition 1 and the additional assumption that the matrices E_ξ and H_w in the corresponding normal form (4) have no elliptic parts. Then the system (3) undergoes, for sufficiently small ε, a Hopf bifurcation at $b = \bar{b} + \varepsilon\mathscr{B} + \mathscr{O}(\varepsilon\sqrt{\varepsilon})$, where $\mathscr{B} = -\chi^{-1}(\bar{f}_m)_y\bar{h}_y\bar{h}_{x_m}/(\bar{f}_m)_y\bar{h}_{x_m}$. This Hopf bifurcation is super(sub)critical if*

$$\frac{1}{2}\mathscr{F}_{uuu} - \mathscr{F}_{uw}H_w^{-1}H_{uu} - \frac{3}{2}\mathscr{F}_{u\xi}E_\xi^{-1}E_{uu} < (>)0. \tag{5}$$

Remark 1. Note that in (5) we corrected the typographical error from [38] where the inequality-signs were listed in an inverted order.

3.2. The normal form reduction

The goal of this section is to bring system (1) to the normal form (4) so that we can verify all hypotheses of Proposition 2. The calculation is algorithmic and we will apply in this context the method introduced in [38]. Before using the normal form reduction algorithm, we need however to make some preparations and write the system in real Jordan form (in fact, in our case, it will be a diagonal form) with respect to the fast variables u_1, u_2 and their fast subsystem (see condition [N0]/ Proposition 1).

The initial step is to write system (1) in slow time $\hat{t} = t/\tau$ and use the notation $\varepsilon = 1/\tau$, that is: $\varepsilon\frac{\mathrm{d}u_j}{\mathrm{d}\hat{t}} = -u_j + S(I - \beta u_k - ga_j)$, $\frac{\mathrm{d}a_j}{\mathrm{d}\hat{t}} = -a_j + u_j$, $(j \neq k; j, k = 1, 2)$. This system has a singular Hopf bifurcation point $\mathbf{e}_H = (u_1^*, a_1^*, u_2^*, a_2^*)$ with $a_1^* = u_1^*$, $a_2^* = u_2^*$ at parameter value I^* defined by equations

$$\begin{cases}\text{(i) } I^* = F(u_1^*) + gu_1^* + \beta u_2^* = F(u_2^*) + gu_2^* + \beta u_1^*,\\ \text{(ii) } F'(u_1^*)F'(u_2^*) = \beta^2.\end{cases} \tag{6}$$

The above conditions for singular Hopf point come from the necessity to have a simple zero eigenvalue in the fast subsystem, that is a simple zero eigenvalue for the upper-left corner two-by-two submatrix in the linearization

$$\mathscr{A} = \begin{pmatrix} -1/\varepsilon & -\beta/(\varepsilon F'(u_1^*)) & -g/(\varepsilon F'(u_1^*)) & 0\\ -\beta/(\varepsilon F'(u_2^*)) & -1/\varepsilon & 0 & -g/(\varepsilon F'(u_2^*))\\ 1 & 0 & -1 & 0\\ 0 & 1 & 0 & -1\end{pmatrix}.$$

Consequently, the fast subsystem component $\mathscr{A}_{(u_1,u_2)}$ of $\mathscr{A}$ possesses two eigenvalues $\lambda_1 = -2/\varepsilon$ and $\lambda_2 = 0$ with corresponding eigenvectors $(\beta, F'(u_1^*))$ and $(-\beta, F'(u_1^*))$. The eigenspace underlies the change of variables $U_1 = \frac{u_1}{2\beta} + \frac{u_2}{2F'(u_1^*)}$, $U_2 = -\frac{u_1}{2\beta} + \frac{u_2}{2F'(u_1^*)}$ and leads to the system

$$\begin{aligned}\varepsilon\frac{\mathrm{d}U_1}{\mathrm{d}\hat{t}} &= -U_1 + \frac{S(I - \beta F'(u_1^*)(U_1 + U_2) - ga_1)}{2\beta}\\ &\quad + \frac{S(I - \beta^2(U_1 - U_2) - ga_2)}{2F'(u_1^*)},\\ \varepsilon\frac{\mathrm{d}U_2}{\mathrm{d}\hat{t}} &= -U_2 - \frac{S(I - \beta F'(u_1^*)(U_1 + U_2) - ga_1)}{2\beta}\\ &\quad + \frac{S(I - \beta^2(U_1 - U_2) - ga_2)}{2F'(u_1^*)},\\ \frac{\mathrm{d}a_1}{\mathrm{d}\hat{t}} &= -a_1 + \beta U_1 - \beta U_2,\\ \frac{\mathrm{d}a_2}{\mathrm{d}\hat{t}} &= -a_2 + F'(u_1^*)U_1 + F'(u_1^*)U_2.\end{aligned} \tag{7}$$

Let us consider now a singular perturbation around the singular Hopf point $\mathbf{e}_H$ at $I = I^*$:

$$I = I^* + \varepsilon\Lambda, \quad (\varepsilon = 1/\tau). \tag{8}$$

For any such perturbation of the parameter I we would like to regularize the system's dynamics to a Λ-independent equilibrium (U_1, U_2, a_1, a_2). We can achieve our goal by rescaling again the time $\hat{t}$ to $s = \hat{t}/\sqrt{\varepsilon}(= t/\sqrt{\tau})$ and by choosing appropriate expansions of the variables:

$$\begin{aligned}U_1 &= \frac{u_1^*}{2\beta} + \frac{u_2^*}{2F'(u_1^*)} + \varepsilon x_1 - \varepsilon\alpha_3\Lambda + \mathscr{O}(\varepsilon^2),\\ a_1 &= a_1^* + \varepsilon y_1 - \varepsilon\alpha_1\Lambda + \mathscr{O}(\varepsilon^2),\\ U_2 &= -\frac{u_1^*}{2\beta} + \frac{u_2^*}{2F'(u_1^*)} + \sqrt{\varepsilon}x_2 - \varepsilon\alpha_4\Lambda + \mathscr{O}(\varepsilon^2),\\ a_2 &= a_2^* + \varepsilon y_2 - \varepsilon\alpha_2\Lambda + \mathscr{O}(\varepsilon^2).\end{aligned} \tag{9}$$

The coefficients α_j, $j = 1, \ldots, 4$, will be determined later such that the $\mathscr{O}(1)$ part of the new system remains independent of Λ, or, equivalently, of the parameter I. Note that the definition of U_2 introduces an additional $\mathscr{O}(\sqrt{\varepsilon})$ term.

The Taylor expansion of the right hand side terms in system (7) take into account the fixed point conditions $S(I^* - ga_1^* - \beta u_2^*) = u_1^*$ and $S(I^* - ga_2^* - \beta u_1^*) = u_2^*$ and use the notation F for the inverse of S $(F = S^{-1})$. Therefore we write $S(I - \beta F'(u_1^*)(U_1 + U_2) - ga_1) = u_1^* + S'(F(u_1^*))X_1 + \frac{1}{2}S''(F(u_1^*))X_1^2 + \frac{1}{6}S'''(F(u_1^*))X_1^3 + h.o.t.$ and $S(I - \beta^2(U_1 - U_2) - ga_2) = u_2^* + S'(F(u_2^*))X_2 + \frac{1}{2}S''(F(u_2^*))X_2^2 + \frac{1}{6}S'''(F(u_2^*))X_2^3 + h.o.t.$ with $X_1 = -\sqrt{\varepsilon}\beta F'(u_1^*)x_2 + \varepsilon\Lambda[1 + g\alpha_1 + \beta F'(u_1^*)\alpha_3 + \beta F'(u_1^*)\alpha_4] - \varepsilon[gy_1 + \beta F'(u_1^*)x_1] + \mathscr{O}(\varepsilon^2)$ and $X_2 = \sqrt{\varepsilon}\beta^2 x_2 + \varepsilon\Lambda[1 + g\alpha_2 + \beta^2\alpha_3 - \beta^2\alpha_4] - \varepsilon[gy_2 + \beta^2 x_1] + \mathscr{O}(\varepsilon^2)$. If we choose α_1, α_2, α_3 and α_4 appropriately (Appendix A), all differential equations will have $\mathscr{O}(1)$ part independent of Λ. Moreover, at the singular Hopf point some additional equalities are true: $F'(u_1^*)F'(u_2^*) = \beta^2$, $S''(F(u_j^*)) = -F''(u_j^*)/F'(u_j^*)^3$ and $S'''(F(u_j^*)) = [3F''(u_j^*)^2 - F'(u_j^*)F'''(u_j^*)]/F'(u_j^*)^5$ for $j = 1, 2$.

After simplifications, we obtain the following equivalent dynamical system

$$\begin{aligned}\sqrt{\varepsilon}\dot{x}_1 &= -2x_1 - \frac{g}{2\beta F'(u_1^*)}y_1 - \frac{g}{2\beta^2}y_2 - \frac{B}{2}x_2^2 + \mathscr{O}(\sqrt{\varepsilon}),\\ \dot{x}_2 &= \frac{g}{2\beta F'(u_1^*)}y_1 - \frac{g}{2\beta^2}y_2 + \frac{A}{2}x_2^2 + \sqrt{\varepsilon}\Big(\gamma\Lambda x_2 + Bx_1x_2\\ &\quad + \frac{gF''(u_1^*)}{2F'(u_1^*)^2}x_2y_1 + \frac{gF''(u_2^*)}{2F'(u_2^*)^2}x_2y_2 + \frac{\tilde{C}}{6}x_2^3\Big) + \mathscr{O}(\varepsilon),\\ \dot{y}_1 &= -\beta x_2 + \sqrt{\varepsilon}(\beta x_1 - y_1) + \mathscr{O}(\varepsilon\sqrt{\varepsilon}),\\ \dot{y}_2 &= F'(u_1^*)x_2 + \sqrt{\varepsilon}(F'(u_1^*)x_1 - y_2) + \mathscr{O}(\varepsilon\sqrt{\varepsilon})\end{aligned} \tag{10}$$

where the dot means differentiation with respect to the new time s $(s = t/\sqrt{\tau})$, $\cdot = \mathrm{d}/\mathrm{d}s$, and the system's coefficients are defined by

$$\begin{aligned}A &= \frac{1}{2\beta\sqrt{F'(u_2^*)}}\left(F'(u_2^*)^{\frac{3}{2}}F''(u_1^*) - F'(u_1^*)^{\frac{3}{2}}F''(u_2^*)\right),\\ B &= \frac{1}{2\beta\sqrt{F'(u_2^*)}}\left(F'(u_2^*)^{\frac{3}{2}}F''(u_1^*) + F'(u_1^*)^{\frac{3}{2}}F''(u_2^*)\right),\\ \gamma &= \frac{1}{4\beta^4\omega^2 + 2\beta^2g^2}[(\beta - g - F'(u_2^*))F'(u_2^*)F''(u_1^*)\\ &\quad + (\beta - g - F'(u_1^*))F'(u_1^*)F''(u_2^*)]\end{aligned} \tag{11}$$

and $\tilde{C} = 3(A^2 + B^2) - \frac{1}{2F'(u_2^*)}\left(F'(u_2^*)^2F'''(u_1^*) + F'(u_1^*)^2F'''(u_2^*)\right)$. Here we used the notation

$$\omega = \sqrt{\frac{g}{2\beta^2}(F'(u_1^*) + F'(u_2^*))}. \tag{12}$$

We transform the system one more time such that to linearly decouple variable x_1 from the slow variables y_1, y_2 while still preserving the diagonal form structure of the subsystem (x_1, x_2). Indeed the change of variables: $y_1 = \tilde{y}_1 - \frac{\varepsilon}{2}\beta\tilde{x}_1$, $y_2 = \tilde{y}_2 - \frac{\varepsilon}{2}F'(u_1^*)\tilde{x}_1$, $x_2 = \tilde{x}_2$ and $x_1 = \tilde{x}_1 - \frac{g}{4\beta F'(u_1^*)}\tilde{y}_1 - \frac{g}{4\beta^2}\tilde{y}_2 + \sqrt{\varepsilon}\left(\frac{gF'(u_1^*)}{8\beta^2} - \frac{g}{8F'(u_1^*)}\right)\tilde{x}_2$ allows us to write (10) in the form

$$
\begin{aligned}
\sqrt{\varepsilon}\dot{\tilde{x}}_1 &= -2\tilde{x}_1 - \frac{B}{2}\tilde{x}_2^2 + \mathcal{O}(\sqrt{\varepsilon}),\\
\dot{\tilde{x}}_2 &= \frac{g}{2\beta F'(u_1^*)}\tilde{y}_1 - \frac{g}{2\beta^2}\tilde{y}_2 + \frac{A}{2}\tilde{x}_2^2\\
&\quad + \sqrt{\varepsilon}\left[\gamma\Lambda\tilde{x}_2 + B\tilde{x}_1\tilde{x}_2 + \left(\frac{gF''(u_1^*)}{2F'(u_1^*)^2} - \frac{gB}{4\beta F'(u_1^*)}\right)\tilde{x}_2\tilde{y}_1\right.\\
&\quad \left. + \left(\frac{gF''(u_2^*)}{2F'(u_2^*)^2} - \frac{gB}{4\beta^2}\right)\tilde{x}_2\tilde{y}_2 + \frac{\tilde{C}}{6}\tilde{x}_2^3\right] + \mathcal{O}(\varepsilon),\\
\dot{\tilde{y}}_1 &= -\beta\tilde{x}_2\\
&\quad + \sqrt{\varepsilon}\left[-\left(1 + \frac{g}{4F'(u_1^*)}\right)\tilde{y}_1 - \frac{g}{4\beta}\tilde{y}_2 - \frac{\beta B}{4}\tilde{x}_2^2\right] + \mathcal{O}(\varepsilon),\\
\dot{\tilde{y}}_2 &= F'(u_1^*)\tilde{x}_2 + \sqrt{\varepsilon}\left[-\frac{g}{4\beta}\tilde{y}_1\right.\\
&\quad \left. - \left(1 + \frac{gF'(u_1^*)}{4\beta^2}\right)\tilde{y}_2 - \frac{F'(u_1^*)B}{4}\tilde{x}_2^2\right] + \mathcal{O}(\varepsilon). \qquad (13)
\end{aligned}
$$

The form of system (13) is now suitable for the singular Hopf normal form method of Braaksma [38] (see also Appendix B). We construct the normal form under the assumption that the coefficient of the quadratic term $\tilde{x}_2^2$ in the second equation is nonzero, that is $A \neq 0$. This is a necessary condition for the reduction.

The calculation is tedious and we refer the reader to [38] for more details. For convenience and clarity, we have also included a list of the important steps in Appendix B. Essentially, we apply a series of smooth transformations to system (13) together with timescaling $\tilde{t} = s\omega$ (that is $\tilde{t} = t\omega/\sqrt{\tau}$ where t is the time in the original equation (1)) in order to obtain the equivalent form

$$
\begin{aligned}
\delta\xi' &= -\frac{2}{\omega^2}\xi + \frac{1}{2}\frac{(-B\omega)}{A}u^2 + \mathcal{O}(\delta),\\
u' &= v + \frac{1}{2}u^2 + \delta\left(\lambda u + \frac{B}{A\omega}u\xi + \frac{g^2D}{A\beta^4}uw + \frac{C}{6}u^3\right) + \mathcal{O}(\delta^2),\\
v' &= -u + \mathcal{O}(\delta^2),\\
w' &= \delta\left(-\left(1 + \frac{g^2}{2\beta^2\omega^2}\right)w + \frac{1}{2}\frac{(-g^2D)}{A\omega^4F'(u_2^*)^2}u^2\right) + \mathcal{O}(\delta^2). \qquad (14)
\end{aligned}
$$

The differentiation is taken with respect to $\tilde{t}$ ($' = \mathrm{d}/\mathrm{d}\tilde{t}$) and the coefficients are $\delta = \sqrt{\varepsilon}/\omega$, A, B, γ and ω defined by (11) and (12), and λ, D and C defined below:

$$
\lambda = \gamma\Lambda - \frac{\beta^2\omega^2(2+\omega^2) - g^2}{2\beta^2\omega^2} \qquad (15)
$$

and

$$
\begin{aligned}
D &= \frac{1}{4}\left(F'(u_2^*)F''(u_1^*) + \beta F''(u_2^*)\right),\\
C &= -\frac{\omega^2}{2A^2F'(u_2^*)}\left(F'(u_2^*)^2F'''(u_1^*) + F'(u_1^*)^2F'''(u_2^*)\right)\\
&\quad - \frac{g^2}{2\beta^2\omega^2} + 1 + \frac{3\omega^2}{2} + \frac{3B^2\omega^2}{A^2}\\
&\quad + \frac{g}{2A\beta F'(u_2^*)^{\frac{1}{2}}}\left(F'(u_2^*)^{\frac{1}{2}}F''(u_1^*) - F'(u_1^*)^{\frac{1}{2}}F''(u_2^*)\right). \qquad (16)
\end{aligned}
$$

This system is in the normal form (4) and have negative coefficients for ξ and w in first and last equations. We conclude that E_ξ and H_w are free of elliptic parts and then apply Proposition 2 to (14). If A and γ are nonzero then the existence of a Hopf bifurcation point in system (1) results immediately; it occurs at a value of parameter I in $\mathcal{O}(\varepsilon)$-distance to I^*.

Let us summarize the result in the following theorem.

Theorem 1. *Consider the critical value of input parameter I^*, and its corresponding values u_1^* and u_2^* according to Eq. (6). If*

$$
\begin{cases}
F'(u_2^*)^{\frac{3}{2}}F''(u_1^*) - F'(u_1^*)^{\frac{3}{2}}F''(u_2^*) \neq 0,\\
(\beta - g - F'(u_2^*))F'(u_2^*)F''(u_1^*)\\
\quad + (\beta - g - F'(u_1^*))F'(u_1^*)F''(u_2^*) \neq 0
\end{cases} \qquad (17)
$$

then, for sufficiently large τ, the system (1) undergoes a Hopf bifurcation at

$$
I_H = I^* + \frac{\beta^2\omega^2(2+\omega^2) - g^2}{(2\gamma\beta^2\omega^2)\tau} + \mathcal{O}\left(\frac{1}{\tau\sqrt{\tau}}\right) \qquad (18)
$$

where γ and ω are defined by (11) and (12) respectively.

Proof. Conditions (17) are equivalent to nonzero A and γ as defined in (11). Therefore we apply Proposition 2 to system (14) and note that $I = I^* + \varepsilon\Lambda$ with $\varepsilon = 1/\tau$. The projection of system (14) onto (u, v) variables has an equilibrium with purely imaginary eigenvalues when λ crosses zero. Clearly, the zero condition for λ is equivalent to $\Lambda = \frac{\beta^2\omega^2(2+\omega^2)-g^2}{2\gamma\beta^2\omega^2}$ (see Eq. (15)) and leads to I_H as above. □

Remark 2. At I_H the nontrivial equilibrium $(u_{1h}, u_{2h}, a_{1h}, a_{2h})$ with $u_{1h} \neq u_{2h}$ satisfies the equalities: $u_{1h} = a_{1h}$, $u_{2h} = a_{2h}$ and $F(u_{1h}) + ga_{1h} + \beta u_{2h} = F(u_{2h}) + gu_{2h} + \beta u_{1h} = I_H$. These conditions are similar to (6) except that the product $F'(u_{1h})F'(u_{2h})$ is no longer equal to β^2. Let us observe that the singular Hopf value I^* can be computed by first determining u_1^* and u_2^* according to the last equality in ((6)-i) together with ((6)-ii), and only then determining I^*. However we cannot apply this strategy to the case of nonsingular ($\varepsilon = 1/\tau$ perturbed) system (1). On the contrary, in system (1) we need to first find I_H from Theorem 1 and only then solve for $(u_{1h}, u_{2h}, a_{1h}, a_{2h})$.

As an example, we computed the singular Hopf point for the choice of parameters as in Fig. 7: $\beta = 2.5, g = 1.5, r = 10, \theta = 0.2$ and $\tau = 5$. From formulas (6) we find $I^* = 3.4016$ and equilibrium $(u_1^*, u_2^*, u_1^*, u_2^*)$ with $u_1^* = 0.99355$, $u_2^* = 0.48302$ close to the transition point from escape to winner-take-all regimes. The hypotheses from Theorem 1 are satisfied ($A = 193.6323$ and $\gamma = 1.7964$ are nonzero) so, according to formula (18), we compute the expected value for the Hopf bifurcation point $I_{sHB} \approx 3.6094$. Since τ is not very large, this result is in quite good agreement with value 3.569 determined in the numerical diagram (Fig. 3). The first Lyapunov coefficient from the normal form is calculated according to formula (5) from Proposition 2 and it is positive (3.8252) implying a subcritical bifurcation (Note that because of the symmetry of the system, another singular Hopf point at I^* is $(u_2^*, u_1^*, u_2^*, u_1^*)$.).

A distinct value $\tilde{I}^*$ that also introduces a singular Hopf in system (1) is found at the transition between release and winner-take-all regimes. It is $\tilde{I}^* = 0.998387$ with $\tilde{u}_1^* = 0.51698$ and $\tilde{u}_2^* = 0.0064489$. In this case γ is negative, but its absolute value is the same as above ($\gamma = -1.7964$). Interesting enough we also found the same value for ω in both situations ($\omega_{I^*} = \omega_{\tilde{I}^*} = 1.3860$); this suggests that not only the product (see condition $F'(u_1^*)F'(u_2^*) = \beta^2$), but also the sum of derivatives $F'(u_1^*)$ and $F'(u_2^*)$ is constant at any singular Hopf for a fixed set of parameters β and g.

4. Neural competition and mixed-mode oscillations

We have seen in Section 3.2 that the occurrence in (1) of the bistable regime between two steady states with, say, $u_1 < u_2$ and $a_j = u_j$ is due to a subcritical Hopf bifurcation. This is the *winner-take-all* state as discussed in [30]. In fact, because of the system's symmetry the two stable equilibria $\mathbf{e}_{il} = (u_{1l}, u_{2l}, a_{1l}, a_{2l})$ and $\mathbf{e}_{sl} = (u_{2l}, u_{1l}, a_{2l}, a_{1l})$ emerge simultaneously, that is at the same value of the parameter $I = I_H$ (see formulas (18), and then (12), (11) for ω and γ). The additional trivial equilibrium point $\mathbf{e}_l = (u_l, u_l, u_l, u_l)$ remains unstable when I crosses the value I_H [30].

The Hopf bifurcation point I_H corresponds to $\lambda = 0$ in the normal form (14). That means that in a neighborhood of I_H, for large enough τ, the local dynamics of (1) around equilibria $\mathbf{e}_{il}$ and $\mathbf{e}_{sl}$ is accurately described by the (u, v)-subsystem. The two-dimensional subsystem is only weakly (linearly) coupled to the rest and at $\lambda = 0$ its trivial equilibrium has a pair of purely imaginary eigenvalues. However, close to the bifurcation point, the linearization in (u, v) has the matrix $\begin{pmatrix} \delta\lambda & 1 \\ -1 & 0 \end{pmatrix}$ with eigenvalues $\frac{\delta\lambda}{2} \pm \mathrm{i}\sqrt{1 - (\frac{\delta\lambda}{2})^2}$. This is an important observation that shows that close to the bifurcation point the eigenvalues have imaginary part of order $\mathcal{O}(1)$ but real part of only $\mathcal{O}(\delta)$ order, or equivalently, of $\mathcal{O}\left(\frac{1}{\omega\sqrt{\tau}}\right)$. We can use the result to explain how subthreshold oscillations as part of MMOs occur in system (1) for certain values of input I close to I_H (Figs. 3 and 7); a construction of the global return map that concatenates trajectories from both slow and fast dynamics leading to MMOs is the subject of a different paper [27].

Let us discuss what happens for values of stimulus strength I, at the transition between the oscillatory regime due to the escape mechanism and the winner-take-all regime (for the transition from release to winner-take-all we will have opposite signs and inequalities in the calculations below; however the conclusion is identical).

By decreasing I through the value I_H the equilibrium points $\mathbf{e}_{il}$ and $\mathbf{e}_{sl}$ change from unstable to stable fixed points. In addition, to the left of I_H an unstable limit cycle of small amplitude appears. Nevertheless the dynamics of the system on the other side (to the right) of I_H just before the bifurcation point is what we would like to investigate. This corresponds to the situation when mixed-mode oscillations are observed in numerical simulations of system (1), Fig. 7.

For $I > I_H$ we have $\Lambda = \tau(I - I^*) = \frac{1}{\varepsilon}(I - I^*) > \frac{\beta^2\omega^2(2+\omega^2)-g^2}{(2\gamma\beta^2\omega^2)}$. We also find that γ is positive which implies, according to definition (15), that so is λ (for example $\gamma = 1.7964$ in the case $I^* = 3.4016$ as discussed in Section 3.2). When the global dynamical map through the relaxation oscillator brings the point in the immediate vicinity of the unstable equilibrium, say, $\mathbf{e}_{il}$, the point is repelled by $\mathbf{e}_{il}$. In the equivalent normal form (14) the equilibrium is the origin and its projection on (u, v)-plane is a focus. Therefore a point starting close to the repelling focus will have a spiral orbit.

In first order approximation, the amplitude of the oscillations is proportional to $\mathrm{e}^{\tilde{t}\frac{\delta\lambda}{2}}$ and starts to significantly increase only when $\tilde{t} = \mathcal{O}(\frac{1}{\lambda\delta})$. Therefore for a fixed λ, in time interval of order $\mathcal{O}(\frac{1}{\delta})$, the trajectory rotates several times around the focus with amplitude approximately constant (or very slow increasing) before the global return map takes it to the neighborhood of the other equilibrium $\mathbf{e}_{sl}$ and vice versa. Moreover the smaller λ is, the slower the increase in amplitude is and so the longer is the time the trajectory spends near the unstable focus. That is consistent with the observation of the increased time spent by the system (1) in either the dominant or suppressed phase of the global relaxation cycle as I approaches I_H (compare Fig. 7A for $I = 3.579$ with Fig. 7B for $I = 3.6$).

While the number of small amplitude oscillations in MMOs is significantly affected by very small changes in I (e.g. 10 peaks at $I = 3.579$ in Fig. 7A, but only 4 peaks at $I = 3.6$ in Fig. 7B), their period is less variable. A rotation around the unstable focus is completed in time $\tilde{t}$ approximately equal to $2\pi/\sqrt{1 - \frac{\delta^2\lambda^2}{4}}$. Expressed in real time t which is related to $\tilde{t}$ by $\tilde{t} = t\omega\sqrt{\varepsilon}$, and using $\delta = \frac{\sqrt{\varepsilon}}{\omega}$, $\varepsilon = \frac{1}{\tau}$ and $\lambda = \tau\gamma(I - I_H)$, the approximate period for the subthreshold oscillations is

$$T_{\mathrm{subthOsc}} \approx \frac{2\pi\sqrt{\tau}}{\omega\sqrt{1 - \frac{\tau\gamma^2}{4\omega^2}(I - I_H)^2}}$$

and it does not change much with I close to I_H. For example, numerical simulations show $T_{\mathrm{subthOsc}} \approx 12.8$ at $I = 3.6$ in Fig. 7B and $T_{\mathrm{subthOsc}} \approx 11.8$ at $I = 3.579$ in Fig. 7A. (To compare, the above formula gives an estimation of $T_{\mathrm{subthOsc}} = 10.147$ for $I = 3.579$.)

5. Discussion

We investigated the occurrence of a complex oscillatory pattern in a reduced firing rate model for two neuronal populations. The network is coupled through direct inhibition, each unit is subject to a slow negative-feedback process in the form of spike frequency adaptation and an external stimulus of equal strength is applied to both populations. For simplicity, adaptation depends linearly on the population activity but the results can be extended to the nonlinear dependency case ($\tau a_j' = -a_j + \sigma(u_j)$ where σ is a sigmoidal function).

The system is generic and has been used in neuroscience to model several experiments such as the central pattern generators [32,34] or perceptual bistability [29–31]. Previous studies [30,31] have classified the types of dynamics in this neuronal competition model into five: fusion at equal activity level, either high or low; rivalry oscillations due to either an escape or a release mechanism; and a winner-take-all behavior. In this paper we show that more complicated trajectories can be found and they appear as the stimulus strength is varied. These trajectories appear at the transition from oscillation to a winner-take-all regime and consist of small amplitude oscillations that alternate with large relaxation-like oscillations during each periodic cycle; they are called *mixed-mode oscillations* (MMOs).

Numerical bifurcation diagrams constructed for the range of stimulus strength close to the transition point reveal several local and global bifurcations such as a double-homoclinic and period-doubling, Neimark–Sacker and limit point bifurcations for cycles. However none of these can consistently and clearly explain the occurrence of MMOs.

We show that the MMOs are associated with a *singular Hopf* bifurcation point. By constructing the normal form at the singular Hopf we propose a mechanism for the formation of subthreshold oscillations in MMOs. Just before the bifurcation that leads to the winner-take-all bistable state, the linearization matrix of the normal form has two complex eigenvalues with positive real part; essentially, however, their real part is $\mathcal{O}\left(\frac{1}{\sqrt{\tau}}\right)$ while their imaginary part is $\mathcal{O}(1)$ as τ takes large values. The main effect of this property is that the orbit of a point in close neighborhood of any of the (unstable) nontrivial equilibria rotates several times around the latter with very slow increasing amplitude. Moreover the closer the parameter is to the transition bifurcation point, the slower the increase in amplitude is. Therefore the point spends longer time near the unstable equilibria before is pushed away through a global map (Fig. 7).

The analysis of the general dynamics, including the switching between the two phases of the relaxation oscillator, needs to take into account the global return map and it is more complicated. However we expect that the singular Hopf point found in system (1) corresponds to a folded saddle–node singularity of type II. This is because previous studies on system (1) show that it has an S-shaped critical manifold with two attractive external branches (say $\mathscr{S}_a$) and one middle repelling branch ($\mathscr{S}_r$) [30]. In addition, on this manifold, the curve of 'jumping' points (the fold curve) is defined by a condition similar to (6), that is $F'(u_1^*)F'(u_2^*) = \beta^2$. As pointed out in [25,28], this is a common situation when a singular Hopf bifurcation point of a slow–fast system is associated with a folded saddle–node singularity. A folded saddle–node singularity of type II is of interest because it allows the reduced flow to cross from the attractive region of the manifold, $\mathscr{S}_a$, to the repelling region $\mathscr{S}_r$ before it switches to a different state through a fast fiber; such trajectories are called *singular canards* and they persist under small perturbations $\varepsilon = \frac{1}{\tau} \ll 1$. The construction of the global return map as part of canard trajectories would prove how the small subthreshold oscillations discussed in Section 4 are concatenated with the fast fibers to form mixed-mode oscillations. We consider it in a future paper [27].

Appendix A. Choice of coefficients α_j in the singular perturbation expansion

The singular perturbation expansion (9) in system (7) leads to the equivalent form (10) with no $\mathscr{O}(1)$ part dependency on Λ if and only if

$$\alpha_1 = \frac{\beta - g - F'(u_2^*)}{2\beta^2\omega^2 + g^2}, \qquad \alpha_2 = \frac{\beta - g - F'(u_1^*)}{2\beta^2\omega^2 + g^2},$$
$$\alpha_3 = \frac{-g(\beta + F'(u_2^*))}{2\beta^2(2\beta^2\omega^2 + g^2)}, \qquad \alpha_4 = \frac{(g - 2\beta)(\beta - F'(u_2^*))}{2\beta^2(2\beta^2\omega^2 + g^2)}.$$

Appendix B. The normal form construction

The system (13) has the form

$$\begin{aligned}
\sqrt{\varepsilon}\dot{\tilde{x}}_1 &= \hat{f}_{x_1}\tilde{x}_1 + \frac{1}{2}\hat{f}_{x_2x_2}\tilde{x}_2^2 + \mathscr{O}(\sqrt{\varepsilon}),\\
\dot{\tilde{x}}_2 &= \bar{f}_y Y + \frac{1}{2}\bar{f}_{xx}\tilde{x}_2^2\\
&\quad + \sqrt{\varepsilon}\left(\alpha\tilde{x}_2 + \bar{f}_{x_1x_2}\tilde{x}_1\tilde{x}_2 + \bar{f}_{xy}\tilde{x}_2 Y + \frac{1}{6}\bar{f}_{xxx}\tilde{x}_2^3\right) + \mathscr{O}(\varepsilon),\\
\dot{Y} &= \bar{h}_x\tilde{x}_2 + \sqrt{\varepsilon}\left(\bar{h}_y Y + \frac{1}{2}\bar{h}_{xx}\tilde{x}_2^2\right) + \mathscr{O}(\varepsilon) \qquad \text{(B.1)}
\end{aligned}$$

with $Y = (\tilde{y}_1, \tilde{y}_2)^T$ and coefficients $\hat{f}_{x_1} = -2$, $\hat{f}_{x_2x_2} = -B$, $\bar{f}_{xx} = A$, $\alpha = \gamma\Lambda$, $\bar{f}_{x_1x_2} = B$, $\bar{f}_{xxx} = \tilde{C}$ and $\bar{f}_y = (\frac{g}{2\beta F'(u_1^*)}, -\frac{g}{2\beta^2})$, $\bar{f}_{xy} = (\frac{gF''(u_1^*)}{2F'(u_1^*)^2} - \frac{gB}{4\beta F'(u_1^*)}, \frac{gF''(u_2^*)}{2F'(u_2^*)^2} - \frac{gB}{4\beta^2})$, $\bar{h}_x = (-\beta, F'(u_1^*))^T$, $\bar{h}_{xx} = (-\frac{\beta B}{2}, -\frac{F'(u_1^*)B}{2})^T$ and

$$\bar{h}_y = \begin{pmatrix} -1 - \dfrac{g}{4F'(u_1^*)} & -\dfrac{g}{4\beta} \\ -\dfrac{g}{4\beta} & -1 - \dfrac{gF'(u_1^*)}{4\beta^2} \end{pmatrix}.$$

At this point we can apply the method introduced by Braaksma [38] and reduce system (13) to the normal form (4).

Note that conditions [N0]–[N5] in Proposition 1 are satisfied. Here the equilibrium point is $\bar{\tilde{x}} = (0, 0)$, $\bar{Y} = (0, 0)$ at value $\bar{\alpha} = 0$ of the parameter α. For example, the linear part in the $\tilde{x}$-subsystem is defined by the matrix $\begin{pmatrix} \hat{f}_{x_1}/\sqrt{\varepsilon} & 0 \\ 0 & \alpha\sqrt{\varepsilon} \end{pmatrix}$ and it leads at $(\bar{\tilde{x}}, \bar{Y}, \bar{\alpha})$ to the matrix $\begin{pmatrix} -2/\sqrt{\varepsilon} & 0 \\ 0 & 0 \end{pmatrix}$ which is in Jordan form. Condition [N3] reduces to $(2\beta^2\omega^2 + g^2)$ which is obviously nonzero and condition [N5] is equivalent to $\bar{f}_y\bar{h}_x = -\omega^2 < 0$. Therefore the reduction to the normal form is possible as long as $A \neq 0$ (see condition [N6] in Proposition 1) and $\gamma \neq 0$ (condition [N7]).

Following the steps in [38] we first introduce a new scalar variable $V = \bar{f}_y Y$ and then change the slow variables Y to $W = Y + \frac{V}{\omega^2}\bar{h}_x$. In this way we obtain two subsystems $\{\tilde{x}_1, \tilde{x}_2, V\}$ and $\{W\}$ that are only weakly ($\mathscr{O}(\sqrt{\varepsilon})$) coupled. Moreover $\tilde{x}_1$ is linearly decoupled from the rest of the system.

A simplification of the $\mathscr{O}(1)$ part of the slow subsystem to a parameterless form results from the scaling $\xi = A\omega\tilde{x}_1$, $\tilde{u} = A\tilde{x}_2/\omega$, $\tilde{v} = AV/\omega^2$, $\tilde{w} = AW/\omega^2$, $\tilde{t} = s\omega$, together with a scaling of the small parameter $\delta = \sqrt{\varepsilon}/\omega$. This is followed by a near-identity transformation that simplifies the $\mathscr{O}(\delta)$ part without any disturbance of the $\mathscr{O}(1)$ terms and by the removal of the $\mathscr{O}(\delta)$ part in the $\tilde{v}$-equation. That is done with the changes $\overline{w} = (\overline{w}_1, \overline{w}_2)^T = \tilde{w} + \delta(\mathbb{I}_2 + \frac{1}{\omega^2}\bar{h}_x\bar{f}_y)\frac{1}{\omega^2}\bar{h}_y\bar{h}_x\tilde{u}$ and $\overline{u} = \tilde{u} - \delta\bar{f}_y(\bar{h}_y\overline{w} - \frac{1}{\omega^2}\bar{h}_y\bar{h}_x\tilde{v} + \frac{1}{2A}\bar{h}_{xx}\tilde{u}^2)$ where $\mathbb{I}_2$ is the two-by-two unit matrix. We should mention that this change of coordinates also replaces the parameter $\alpha = \gamma\Lambda$ by $\lambda = \gamma\Lambda - \frac{1}{\omega^2}\bar{f}_y\bar{h}_y\bar{h}_x$.

We can remove the $\overline{u}\tilde{v}$ quadratic term in the $\overline{u}$-equation with the change $u = \overline{u} + \frac{1}{3}\delta\Omega(\frac{1}{2}\overline{u}^2\tilde{v} - \overline{u}^2 + \tilde{v}^2)$ and $v = \tilde{v} - \frac{1}{3}\delta\Omega\overline{u}\tilde{v}$ where $\Omega = -(\frac{1}{\omega^2}\bar{f}_y\bar{h}_y\bar{h}_x + \frac{1}{A}\bar{f}_{xy}\bar{h}_x + \frac{1}{A}\bar{f}_y\bar{h}_{xx})$.

The last step is to eliminate one of the two variables in the vector $\overline{w}$ which is certainly superfluous. That is because we introduced V (and so v) as a new scalar variable to the original system but also kept all others. We note that $\bar{f}_y W = \bar{f}_y Y + \frac{V}{\omega^2}\bar{f}_y\bar{h}_x = V(1 + \frac{1}{\omega^2}(-\omega^2)) = 0$ implies $\overline{w}_2 = \frac{\beta}{F'(u_1^*)}\overline{w}_1 + \mathscr{O}(\delta)$. Therefore we define the scalar $w = \overline{w}_1$; then we discard the equation for $\overline{w}_2$ while keeping only that of $\overline{w}_1$ with the appropriate changes. System (14) results immediately.

References

[1] J. Hudson, M. Hart, D. Marinko, An experimental study of multiple peak periodic and nonperiodic oscillations in the Belousov–Zhabotinskii reaction, J. Chem. Phys. 71 (1979) 1601–1606.
[2] V. Petrov, S.K. Scott, K. Showalter, Mixed-mode oscillations in chemical systems, J. Chem. Phys. 97 (9) (1992) 6191–6198.
[3] K. Krischer, M. Lübke, M. Eiswirth, W. Wolf, J.L. Hudson, G. Ertl, A hierarchy of transitions to mixed mode oscillations in an electrochemical system, Physica D 62 (1993) 123–133.
[4] I.R. Epstein, K. Showalter, Nonlinear chemical dynamics: Oscillations, patterns, and chaos, J. Phys. Chem. 100 (1996) 13132–13147.
[5] V.K. Vanag, L. Yang, M. Dolnik, A.M. Zhabotinsky, I.R. Epstein, Oscillatory cluster patterns in a homogeneous chemical system with global feedback, Nature 406 (2000) 389–391.
[6] V.K. Vanag, A.M. Zhabotinsky, I.R. Epstein, Pattern formation in the Belousov–Zhabotinsky reaction with photochemical global feedback, J. Phys. Chem. A 104 (2000) 11566–11577.
[7] K. Kovacs, M. Leda, V.K. Vanag, I.R. Epstein, Small-amplitude and mixed-mode pH oscillations in the bromate-sulfite-ferrocyanide-aluminum(III) system, J. Phys. Chem. A 113 (2009) 146–156.
[8] T. Hayashi, Mixed-mode oscillations and chaos in a glow discharge, Phys. Rev. Lett. 84 (2000) 3334–3337.
[9] M. Mikikian, M. Cavarroc, L. Couedel, Y. Tessier, L. Boufendi, Mixed-mode oscillations in complex-plasma instabilities, Phys. Rev. Lett. 100 (2008) 1–4. 225005.
[10] A.A. Alonso, R.R. Llinás, Subthreshold Na^+-dependent theta like rhythmicity in stellate cells of entorhinal cortex layer II, Nature 342 (1989) 175–177.
[11] C.A. Del Negro, C.G. Wilson, R.J. Butera, H. Rigatto, J.C. Smith, Periodicity, mixed-mode oscillations, and quasiperiodicity in a rhythm-generating neural network, Biophys. J. 82 (2002) 206–214.
[12] G. Medvedev, J.E. Cisternas, Multimodal regimes in a compartmental model of the dopamine neuron, Physica D 194 (3–4) (2004) 333–356.
[13] A. Kuznetsov, N. Kopell, C. Wilson, Transient high-frequency firing in a coupled-oscillator model of the mesencephalic dopaminergic neuron, J. Neurophysiol. 95 (2006) 932–947.
[14] J. Rubin, M. Wechselberger, The selection of mixed-mode oscillations in a Hodgkin–Huxley model with multiple timescales, Chaos 18 (2008) 1–12, 015105.

[15] B. Ermentrout, M. Wechselberger, Canards, clusters and synchronization in a weakly coupled interneuron model, SIAM J. Appl. Dyn. Syst. 8 (1) (2009) 253–278.
[16] H. Rotstein, M. Wechselberger, N. Kopell, Canard induced mixed-mode oscillations in a medial entorhinal cortex layer II stellate cell model, SIAM J. Appl. Dyn. Syst. 7 (2008) 1582–1611.
[17] L. Shilnikov, A. Shilnikov, Shilnikov bifurcation, Scholarpedia 2 (8) (2007) 1981.
[18] M.T.M. Koper, Bifurcations of mixed-mode oscillations in a three-variable autonomous Van der Pol–Duffing model with a cross-shaped phase diagram, Physica D 80 (1995) 72–94.
[19] R. Larter, C. Steinmetz, Chaos via mixed-mode oscillations, Phil. Trans. R. Soc. London A 337 (1991) 291–298.
[20] J. Guckenheimer, A. Willms, Asymptotic analysis of subcritical Hopf-homoclinic bifurcation, Physica D 139 (2000) 195–216.
[21] P. Szmolyan, M. Wechselberger, Canards in $\mathbb{R}^3$, J. Differential Equations 177 (2001) 419–453.
[22] M. Brons, M. Krupa, M. Wechselberger, Mixed mode oscillations due to the generalized canard phenomenon, Fields Inst. Commun. 49 (2006) 39–63.
[23] H. Rotstein, N. Kopell, A.M. Zhabotinsky, I.R. Epstein, Canard phenomenon and localization of oscillations in the Belousov–Zhabotinsky reaction with global feedback, J. Chem. Phys. 119 (2003) 8824–8832.
[24] J. Drover, J. Rubin, J. Su, B. Ermentrout, Analysis of a canard mechanism by which excitatory synaptic coupling can synchronize neurons at low firing frequencies, SIAM J. Appl. Math. 62 (1) (2004) 69–92.
[25] J. Guckenheimer, Singular Hopf bifurcation in systems with two slow variables, SIAM J. Appl. Dyn. Syst. 7 (4) (2008) 1355–1377.
[26] M. Wechselberger, Existence and bifurcation of canards in $\mathbb{R}^3$ in the case of a folded node, SIAM J. Applied Dynamical Systems 4 (2005) 101–139.
[27] R. Curtu, J. Rubin, Canards and folded saddle-node singularities of type II in a reduced firing rate inhibitory network, Chaos (2010) (submitted for publication).
[28] M. Krupa, M. Wechselberger, Local analysis near a folded saddle-node singularity (2008), preprint.
[29] C.R. Laing, C.C. Chow, A spiking neuron model for binocular rivalry, J. Comput. Neurosci. 12 (2002) 39–53.
[30] R. Curtu, A. Shpiro, N. Rubin, J. Rinzel, Mechanisms for frequency control in neuronal competition models, SIAM J. Appl. Dyn. Syst. 7 (2) (2008) 609–649.
[31] A. Shpiro, R. Curtu, J. Rinzel, N. Rubin, Dynamical characteristics common to neuronal competition models, J. Neurophysiol. 97 (2007) 462–473.
[32] R.L. Calabrese, Half-center oscillators underlying rhythmic movements, in: M.A. Arbib (Ed.), The Handbook of Brain Theory and Neural Networks, MIT Press, Cambridge, MA, 1995, pp. 444–447.
[33] F.K. Skinner, N. Kopell, E. Marder, Mechanisms for oscillation and frequency control in reciprocally inhibitory model neural networks, J. Comput. Neurosci. 1 (1994) 69–87.
[34] A.L. Taylor, G.W. Cottrell, W.B. Kristan, Analysis of oscillations in a reciprocally inhibitory network with synaptic depression, Neural Comput. 14 (2002) 561–581.
[35] B. Ermentrout, Simulating, analyzing, and animating dynamical systems: A guide to XPPAUT for researchers and students, in: Software Environ. Tools, vol. 14, SIAM, Philadelphia, 2002.
[36] B. Ermentrout, http://www.math.pitt.edu/~bard/xpp/xpp.html.
[37] A. Dhooge, W. Govaerts, Yu.A. Kuznetsov, MATCONT: A Matlab package for numerical bifurcation analysis of ODEs, ACM Trans. Math. Software 29 (2003) 141–164. http://www.matcont.ugent.be/.
[38] B. Braaksma, Singular Hopf bifurcation in systems with fast and slow variables, J. Nonlinear Sci. 8 (1998) 457–490.